arXiv:1607.04943v1 [cond-mat.mes-hall] 18 Jul 2016

Magneto-conductivities in Weyl semimetals: the effect of chemical potential and temperature

Xiao Xiao[1], K. T. Law[1] and P. A. Lee[2,*]

[1]*Department of Physics, The Hong Kong University of Science and Technology, Hong Kong, Peoples Republic of China*

[2]*Department of Physics, Massachusetts Institute of Technology, Cambridge, Massachusetts 02139, USA*

(Dated: July 19, 2016)

We present the detailed analyses of magneto-conductivities in a Weyl semimetal within Born approximation. In the presence of the charged impurities, the linear magnetoresistance can happen when the chemical potential intersects only with the zeroth (n=0) Landau level. Interestingly, the linear magnetoresistance is very robust against the change of temperature, when chemical potential is within this regime. On the other hand, the linear magnetoresistance disappears once the chemical potential can cut the higher Landau levels. Our analysis indicates that the deviation from the linear magnetoresistance is mainly due to the behavior change of the longitudinal conductivity. Within this regime of chemical potential, the behavior of longitudinal conductivity shows very clear temperature dependence. As a consequence, the magnetoresistance obtained within the self-energy approximation shows a non-monotonous behavior with the increment of magnetic field, which is inconsistent with experimental results. We thus conclude that the Born approximation treatment of the problem does not explain the recent experimental observation of linear magnetoresistance.

*Electronic address: palee@mit.edu

I. INTRODUCTION

Properties of gapless Dirac fermions attract much attention in the community, since the successful fabrication of monolayer graphene [1]. Its dispersion spectrum is characterized by two Dirac points at which the conduction band and valance band touch. Importantly, The Dirac points in graphene are stabilized by symmetries with a $\pm\pi$ Berry phase, as long as both the time reversal and inversion symmetry are present. Due to the Dirac dispersion spectrum, graphene has been a novel platform to explore interesting physics in two-dimension, such as the novel properties of collective modes [2], unconventional effects of interactions and disorders [2–4], and the exciting properties under magnetic field [5, 6].

Very recently, three-dimension Dirac Fermions are predicted [7, 8] to be harbored in Na_3Bi and Cd_3As_2, and it was verified later in the angle-resolved photoemission spectroscopy (ARPES) experiments [9]. The Dirac semimetal phase in these materials is stabilized by the time reversal and the inversion symmetry together with crystalline symmetry [10], so the low energy physics around the Dirac point is described at least by a 4×4 matrix and the conduction and valence bands are two-fold degeneracy. When the time reversal or inversion symmetry is broken, the two Dirac points in these materials would be split into two pairs of Weyl points with opposite chirality. In this sense, the Weyl semimetal is robust and does not depends on any symmetry (except for the translation symmetry in the crystal). Recently, ARPES experiments had identified the Weyl semimetal phase in TaAs [11] and NbAs [12]. In addition to materials belong to the same family of TaAs and NbAs [13], the pyrochlore iridates [14] and topological insulator heterostructures [15] are predicted to harbor Weyl femrions. To conserve the total chirality, the Weyl points should appear in pairs with opposite chirality, which thus leads to the chiral anomaly (or the Adler-Bell-Jackiw anomaly)

[16, 17]. It indicates that the electrons can be pumped from one node to the other with opposite chirality at a rate proportional to $\vec{E} \cdot \vec{B}$ [18–21], when applying the electric field parallel to the external magnetic fields. Therefore, the observation of the negative magnetoresistance is expected to be a signature of chiral anomaly [22]. However, there are unexpected phenomena under external magnetic field in addition to the chiral anomaly. Very strikingly and interestingly, in the recent experiments [23–26], in the configuration that the magnetic field is perpendicular to the electric field, a linear and non-saturated magnetoresistence is observed in the Dirac semimetals. This is in contrast to the standard relaxation time analysis of the Boltzmann equation, where the resistivity saturates for $\omega_c\tau \gg 1$ where ω_c is the cyclotron frequency and τ is the relaxation time.

The early work of Abrikosov was among the few examples where linear magnetoresistance was predicted in a single band system [27]. Abrikosov showed that in a Dirac electronic spectrum, when the chemical potential coincides with the zeroth Landau level, linear magnetoresistance is obtained in the Born approximation in a model with long range changed impurities scattering. Recent papers [28, 30] have re-examined this problem in detail. In particular, ref.[28] showed that Coulomb impurity is crucial for the linear magnetoresistance found by Abrikosov. Meanwhile, Song *et al* [29] approached problem from the point of view of the classical motion of guiding center in the case of random potential which is slowly varying in space. In the case where the cyclotron orbit size is smaller than the distance scale of the variation of the random potential, they showed that linear magnetoresistance is obtained even when the chemical potential is far away from the Dirac neutrality point.

Motivated by these experimental observations and the early work of Abrikosov [27], in this work we calculate the magneto-conductivities in a Weyl semimetal in the presence of charged impurities, which are crucial for the appearance of linear magnetoresistance within the self-energy approximation adopted here [28, 30]. The detailed analyses clarify

how the chemical potential and temperature affect the behaviors of the magneto-conductivities within the framework of Born approximation. In our analysis, we assumed that the system is with a given carrier density. Then the chemical potential can intersect with only the zeroth Landau level, when the magnetic field is large enough. In this regime of chemical potential, both Hall and longitudinal conductivities are inversely proportional to magnetic field ($1/B$ behaviors), and thus the system shows the linear magnetoresistance. Moreover, we show that the $1/B$ behaviors for conductivities are very robust against the change of temperature, as long as the chemical potential is kept in this regime. On the other hand, by decreasing the magnetic field, the chemical potential can cross higher Landau levels. When this happens, the Hall conductivity shows a slight deviation from the $1/B$ behavior. In the contrast, the change of longitudinal conductivity is dramatic and temperature dependent. When the temperature is low (much smaller than the typical gap between Landau levels $T \ll \sqrt{v^2 eB/c}$), the change of the longitudinal conductivity with the decreasing magnetic field shows a 'step-like' structure. Moreover, due to the high density of states at the edges of Landau levels, a local maximal in longitudinal conductivity appears accordingly. When the temperature is comparable to $\sqrt{v^2 eB/c}$, the longitudinal conductivity shows the monotonous power law increasing with the decreasing magnetic field ($\sim 1/B^n$). The power n first increases with the number of the involved Landau levels. After arriving at its maximum $n \approx 3$, the power n decrease again. Finally when the magnetic field is small enough, the dependence of the longitudinal conductivity with the magnetic field shows a Lorentzian form, recovering the Boltzmann results. Then the magnetoresistance ρ_{xx} can be obtained from the longitudinal and Hall conductivity within the self-energy approximation, and it turns out to manifest a complex non-monotonous increment with the magnetic field. However, in the experiment the chemical potential is generally far from the neutrality point, and the magnetoresistance ρ_{xx} increases with magnetic field monotonously. We therefore conclude that the Born approximation treatment of this

work does not explain the experimental observations of linear magnetoresistance in Weyl semimetals. Presumably the results of Song *et al* [29] are in a limit where the Born approximation is not valid, thus explaining the different conditions of the two treatments.

In what follows, we begin with the introduction of model and give a brief outline of the method in section II. In Section III, the numerical results under both the low temperature and high temperature are first present and discussed. Then we analyze the behavior of magnetoresistance ρ_{xx} obtained within the Born approximation and make a comparison with the experimental results from ref.[26]. Finally, a summary of the results are made in section IV.

II. MODEL AND METHOD

Our discussion begins with the low energy effective Hamiltonian for a single Weyl node. In this section, we outline the theoretical framework to study the magneto-conductivities. First we give explanations for the Hamiltonian of the system and give the explicit form of the Matsubara Green's function, and then based on the Matsubara Green's function we derive the expressions for the magneto-conductivities.

A. Hamiltonian and Matsubara Green's function

Usually the Weyl node should appear in pairs, but it is still valid to consider only one Weyl node at a time, if the energy scale of interest is much lower than the Lifshitz point. Then under external magnetic field the system is described by the following effective Hamiltonian:

$$H\left(\vec{k}\right)=\int d^{3}r\psi^{\dagger}\left(\vec{r}\right)v\vec{\sigma}\cdot\left(\vec{k}-\frac{e}{c}\vec{A}\right)\psi\left(\vec{r}\right), \tag{1}$$

where $\vec{\sigma}$ is the Pauli matrices, $\vec{A}$ is the vector potential induced by the magnetic field, and v is the Fermi velocity. We assume that the external magnetic field is along the z-direction, and choose the gauge that the vector potential takes the form $\vec{A} = (0, Bx, 0)$. From the Hamiltonian Eq.(1), the Landau level energies can be solved:

$$E_n^{\pm} = \pm v\sqrt{k_z^2 + 2n\beta_0}, \tag{2}$$

where we have defined $\beta_0 = eB/c$. The corresponding Landua level wave functions are given by:

$$\psi_n^+ = \sqrt{\frac{1}{2}} \begin{pmatrix} \chi_n^+ (k_z, \beta_0)\, \phi_n \\ \\ -i\chi_n^- (k_z, \beta_0)\, \phi_{n-1} \end{pmatrix},$$

$$\psi_n^- = \sqrt{\frac{1}{2}} \begin{pmatrix} \chi_n^- (k_z, \beta_0)\, \phi_n \\ \\ i\chi_n^+ (k_z, \beta_0)\, \phi_{n-1} \end{pmatrix}, \tag{3}$$

where $\chi_n^+ (k_z, \beta_0) = \sqrt{\left(1 + \frac{k_z}{\sqrt{k_z^2+2n\beta_0}}\right)}$, $\chi_n^- (k_z, \beta_0) = \sqrt{\left(1 - \frac{k_z}{\sqrt{k_z^2+2n\beta_0}}\right)}$, and $\phi_n (\tilde{x})$ is the usual eigenfunction of harmonic oscillator and of the form:

$$\phi_n (\tilde{x}) = \sqrt{\frac{\sqrt{\beta_0}}{(2^n n!)\sqrt{\pi}}} \exp\left(\frac{-\beta_0}{2\tilde{x}^2}\right) H_n\left(\sqrt{\beta_0}\tilde{x}\right). \tag{4}$$

In the above, we have defined $\tilde{x} = x - k_y/\beta_0$. Then we can define the Matsubara Green's function as:

$$\tilde{G}_0 (k_z, k_y, x, x', \omega_m) = \sum_{n,\gamma=\pm} \frac{\psi_n^\gamma (x - k_y/\beta_0)\, \psi_n^{\gamma\,\dagger} (x' - k_y/\beta_0)}{i\omega_m + \mu - E_n^\gamma (k_z)}, \tag{5}$$

where $\tilde{G}_0$ denotes the Green's function matrix under the representation of Pauli matrices in the original Hamiltonian.

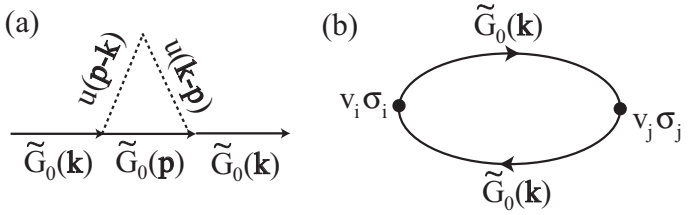

FIG. 1: (a) the diagrammatic expression of Born approximation for the self-energy due to the charge impurities; (b) the diagrammatic expression of the magneto-conductivity σ_{ij}. In the figure, the solid line denotes the Green's function, the dashed line denotes the impurity scattering, and the dot denotes the velocity vertex.

B. The charged impurities

As we had mentioned, the presence of the charged impurities is crucial for the appearance of linear magnetoresistance within the self-energy approximation. In this case, the impurity scattering potential is given by:

$$u\left(\vec{k}\right)=\frac{4\pi e^{2}}{\varepsilon_{\infty}\left(k^{2}+\kappa^{2}\right)}, \tag{6}$$

where ε_{∞} indicates the background dielectric constant, and the inverse of the screening length κ is given by:

$$\begin{aligned}\kappa^{2}&=\frac{4\pi e^{2}}{\varepsilon_{\infty}}\frac{1}{V}\sum_{n,\lambda}\int_{0}^{\beta}d\tau\left\langle T_{\tau}\varrho_{n}^{\lambda}\left(\tau\right)\left(\varrho_{n}^{\lambda}\right)^{\dagger}\left(0\right)\right\rangle\\&=\frac{2e^{2}\beta}{\pi\varepsilon_{\infty}}\sum_{n,\lambda}\int dk_{z}\frac{dn_{n}^{\lambda}\left(vk_{z}\right)}{d\mu},\end{aligned} \tag{7}$$

where ϱ_{n}^{λ} is the density operator for the λn Landau level, and $n_{n}^{\lambda}\left(vk_{z}\right)$ is the Fermi-Dirac distribution for the λn Landau level. Then within the Born approximation (see Fig. 1(a)), the relaxation time for the Landau level E_{n}^{λ} is

given by:

$$\frac{1}{\tau_n^\lambda(k_z)} = \frac{e^4}{\varepsilon_\infty^2}\frac{N_i}{v}\sum_{\gamma=\pm}\int d(vk_z')\Big\{\frac{T}{\left(\mu - E_{n-1}^\gamma\left(k_z'\right)\right)^2+T^2}\left[\frac{(\mathcal{B}_{n,\lambda}^{n-1,\gamma}\left(k_z,k_z'\right))^2}{\beta_0^2}+(\mathcal{A}_{n,\lambda}^{n-1,\gamma}\left(k_z,k_z'\right))^2\right]$$
$$\times\left(\ln\frac{\beta_0+K^2(k_z,k_z')}{K^2(k_z,k_z')}+\frac{K^2(k_z,k_z')}{\beta_0+K^2(k_z,k_z')}-1\right)\Big\}$$
$$+\frac{e^4}{\varepsilon_\infty^2}\frac{N_i}{v}\sum_{\gamma=\pm}\int d(vk_z')\Big\{\frac{T}{\left(\mu - E_{n+1}^\gamma\left(k_z'\right)\right)^2+T^2}\left[\frac{(\mathcal{B}_{n,\lambda}^{n+1,\gamma}\left(k_z,k_z'\right))^2}{\beta_0^2}+(\mathcal{A}_{n,\lambda}^{n+1,\gamma}\left(k_z,k_z'\right))^2\right]$$
$$\times\left(\ln\frac{\beta_0+K^2(k_z,k_z')}{K^2(k_z,k_z')}+\frac{K^2(k_z,k_z')}{\beta_0+K^2(k_z,k_z')}-1\right)\Big\}, \tag{8}$$

where $T = k_B T$ presents the thermal energy, N_i is the density of charge impurities, μ is the chemical potential, and we have defined $K^2(k_z,k_z') = \left(k_z - k_z'\right)^2 + \kappa^2$ for the convenience. In the above derivation, we have used the thermal energy T to regularize the singularity of the Matsubara Green's function and account the effect of temperature around the Fermi surface. The functions $\mathcal{A}$ and $\mathcal{B}$ are defined as following:

$$\mathcal{A}_{n,\lambda}^{m,\gamma}\left(k_z,k_z'\right) = \int dx\left(\psi_n^\lambda\right)^\dagger x\psi_m^\gamma, \tag{9}$$

$$\mathcal{B}_{n,\lambda}^{m,\gamma}\left(k_z,k_z'\right) = \int dx\left(\psi_n^\lambda\right)^\dagger \partial_x\psi_m^\gamma, \tag{10}$$

where ψ_n^λ is the wave function of the Landau level E_n^λ given in Eq.(3).

C. The magneto-conductivities

As usual, the conductivities can be related to the Q-matrix, which is given by (Fig. 1(b)):

$$Q_{ij}\left(i\omega\right) = \frac{2e^2v^2T}{c}\sum_m\int\frac{dk_y}{2\pi}\frac{dk_z}{2\pi}dx'\mathrm{Tr}\left[\sigma_i\tilde{G}_0\left(k_z,k_y,x,x',\omega_m+\omega\right)\sigma_j\tilde{G}_0\left(k_z,k_y,x,x',\omega_m\right)\right]. \tag{11}$$

Then the static conductivities can be obtained from:

$$\sigma_{ij} = \lim_{\omega\to 0}\frac{icQ_{ij}^R\left(\omega\right)}{\omega}, \tag{12}$$

where the superscript R denotes to take the retarded part of the Q-matrix.

In this work, we focus on the case when the density of the charged impurities is low ($1/\tau_n^{\lambda} \ll \sqrt{v^2\beta_0}$). Under the assumption, the Hall conductivity is given by:

$$\begin{aligned}
\sigma_{xy} = & \frac{-e^2v^2\beta_0}{4\pi}\int\frac{dk_z}{2\pi}\sum_{n=1}\left[\tanh\frac{E_{n-1}^{+}(k_z)-\mu}{2T}-\tanh\frac{E_{n}^{+}(k_z)-\mu}{2T}\right]\frac{\left(\chi_n^{-}(k_z)\right)^2\left(\chi_{n-1}^{+}(k_z)\right)^2}{\left(E_{n-1}^{+}(k_z)-E_n^{+}(k_z)\right)^2} \\
& + \frac{-e^2v^2\beta_0}{4\pi}\int\frac{dk_z}{2\pi}\sum_{n=1}\left[\tanh\frac{E_{n-1}^{-}(k_z)-\mu}{2T}-\tanh\frac{E_{n}^{+}(k_z)-\mu}{2T}\right]\frac{\left(\chi_n^{-}(k_z)\right)^2\left(\chi_{n-1}^{-}(k_z)\right)^2}{\left(E_{n-1}^{-}(k_z)-E_n^{+}(k_z)\right)^2} \\
& + \frac{-e^2v^2\beta_0}{4\pi}\int\frac{dk_z}{2\pi}\sum_{n=1}\left[\tanh\frac{E_{n-1}^{+}(k_z)-\mu}{2T}-\tanh\frac{E_{n}^{-}(k_z)-\mu}{2T}\right]\frac{\left(\chi_n^{+}(k_z)\right)^2\left(\chi_{n-1}^{+}(k_z)\right)^2}{\left(E_{n-1}^{+}(k_z)-E_n^{-}(k_z)\right)^2} \\
& + \frac{-e^2v^2\beta_0}{4\pi}\int\frac{dk_z}{2\pi}\sum_{n=1}\left[\tanh\frac{E_{n-1}^{-}(k_z)-\mu}{2T}-\tanh\frac{E_{n}^{-}(k_z)-\mu}{2T}\right]\frac{\left(\chi_n^{+}(k_z)\right)^2\left(\chi_{n-1}^{-}(k_z)\right)^2}{\left(E_{n-1}^{-}(k_z)-E_n^{-}(k_z)\right)^2}. \qquad (13)
\end{aligned}$$

Similarly, the longitudinal conductivity is given by:

$$\sigma_{xx} = \frac{2e^2v^2}{T}\frac{\beta_0}{2\pi}\int\frac{d\omega}{2\pi}\frac{dk_z}{2\pi}\cosh^{-2}\frac{\omega}{2T}F(\omega,k_z), \qquad (14)$$

where

$$\begin{aligned}
F(\omega,k_z) = & \frac{1}{4}\sum_n\frac{\left(\chi_n^{-}(k_z,B)\right)^2/\tau_n^{+}}{\left(\omega+\mu-E_n^{+}(k_z)\right)^2+\frac{1}{(\tau_n^{+})^2}}\frac{\left(\chi_{n-1}^{+}(k_z,B)\right)^2/\tau_{n-1}^{+}}{\left(\omega+\mu-E_{n-1}^{+}(k_z)\right)^2+\frac{1}{(\tau_{n-1}^{+})^2}} \\
& + \frac{1}{4}\sum_n\frac{\left(\chi_n^{-}(k_z,B)\right)^2/\tau_n^{+}}{\left(\omega+\mu-E_n^{+}(k_z)\right)^2+\frac{1}{(\tau_n^{+})^2}}\frac{\left(\chi_{n-1}^{-}(k_z,B)\right)^2/\tau_{n-1}^{-}}{\left(\omega+\mu-E_{n-1}^{-}(k_z)\right)^2+\frac{1}{(\tau_{n-1}^{-})^2}} \\
& + \frac{1}{4}\sum_n\frac{\left(\chi_n^{+}(k_z,B)\right)^2/\tau_n^{-}}{\left(\omega+\mu-E_n^{-}(k_z)\right)^2+\frac{1}{(\tau_n^{-})^2}}\frac{\left(\chi_{n-1}^{+}(k_z,B)\right)^2/\tau_{n-1}^{+}}{\left(\omega+\mu-E_{n-1}^{+}(k_z)\right)^2+\frac{1}{(\tau_{n-1}^{+})^2}} \\
& + \frac{1}{4}\sum_n\frac{\left(\chi_n^{+}(k_z,B)\right)^2/\tau_n^{-}}{\left(\omega+\mu-E_n^{-}(k_z)\right)^2+\frac{1}{(\tau_n^{-})^2}}\frac{\left(\chi_{n-1}^{-}(k_z,B)\right)^2/\tau_{n-1}^{-}}{\left(\omega+\mu-E_{n-1}^{-}(k_z)\right)^2+\frac{1}{(\tau_{n-1}^{-})^2}}. \qquad (15)
\end{aligned}$$

D. chemical potential

In this work, we assume that the carrier density of the system is given. Then for a given magnetic field, the chemical potential can be determined easily. By tuning the strength of magnetic field, the system can be tuned to different regimes of chemical potential. Supposing the carrier density is n_0, the chemical potential can be determined from the following equation:

$$\frac{\beta_0}{\pi}\left[\int_0^\infty\left(\frac{dk_z}{e^{(E_0^+(k_z)-\mu)/T}+1}-\frac{dk_z}{e^{(E_0^+(k_z)+\mu)/T}+1}\right)+\sum_{n=1}\int_{-\infty}^\infty\left(\frac{dk_z}{e^{(E_n^+(k_z)-\mu)/T}+1}-\frac{dk_z}{e^{(E_n^+(k_z)+\mu)/T}+1}\right)\right]=n_0, \tag{16}$$

where $E_n^+(k_z)=\sqrt{v^2k_z^2+2nv^2\beta_0}$. The first term can be integrated out exactly, so we end up with:

$$\frac{\beta_0}{\pi}\left[\frac{\mu}{v}+\sum_{n=1}\int_{-\infty}^\infty\left(\frac{dk_z}{e^{(E_n^+(k_z)-\mu)/T}+1}-\frac{dk_z}{e^{(E_n^+(k_z)+\mu)/T}+1}\right)\right]=n_0. \tag{17}$$

III. RESULTS AND DISCUSSION

With the formulas obtained in the last section, we calculate the magneto-conductivity under different conditions. The following two conditions are considered: 1. the thermal energy is much smaller than the typical gap between Landau levels ($T\ll\sqrt{v^2\beta_0}$); 2. the thermal energy is comparable with the typical gap between Landau levels ($T\sim\sqrt{v^2\beta_0}$)). Here we are interested in the clean limit: $\tau_n^\lambda\ll\sqrt{v^2\beta_0}$, so that the smearing of the Landau level is mainly due to the importance of temperature. To avoid difficulties in calculations, the carrier density is justified so that there are not too many Landau levels involving the calculations. Moreover, for the convenience of calculations, we choose the thermal energy T as the energy unit and normalize all the quantities according to the thermal energy T. Then we have a set of dimensionless normalized quantities: $\tilde{k}=vk_z/T$, $\tilde{\mu}=\mu/T$ and $\tilde{\beta}=2v^2\beta_0/T^2$.

By using the normalized quantities, the equation determining the chemical potential becomes:

$$\tilde{\beta}\left[\tilde{\mu}+\sum_{n=1}^{N}\int_{-\infty}^{\infty}\left(\frac{d\tilde{k}_z}{e^{(E_n^+(\tilde{k}_z,\tilde{\beta})-\tilde{\mu})}+1}-\frac{d\tilde{k}_z}{e^{(E_n^+(\tilde{k}_z,\tilde{\beta})+\tilde{\mu})}+1}\right)\right]=\frac{2\pi v^3 n_0}{T^3}. \tag{18}$$

We can likewise define the dimensionless normalized carrier density $\tilde{n}_0=\frac{2\pi v^3 n_0}{T^3}$. Also the Hall conductivity and longitudinal conductivity can be expressed by using these normalized quantities:

$$\begin{aligned}
\sigma_{xy}=&\frac{-e^2\tilde{\beta}T}{16\pi^2 v}\int d\tilde{k}\sum_{n=1}\left[\tanh\frac{\tilde{E}_{n-1}^{+}\left(\tilde{k}\right)-\tilde{\mu}}{2}-\tanh\frac{\tilde{E}_{n}^{+}\left(\tilde{k}\right)-\tilde{\mu}}{2}\right]\frac{\left(\chi_n^-\left(\tilde{k}\right)\right)^2\left(\chi_{n-1}^+\left(\tilde{k}\right)\right)^2}{\left(\tilde{E}_{n-1}^{+}\left(\tilde{k}\right)-\tilde{E}_{n}^{+}\left(\tilde{k}\right)\right)^2}\\
&+\frac{-e^2\tilde{\beta}T}{16\pi^2 v}\int d\tilde{k}\sum_{n=1}\left[\tanh\frac{\tilde{E}_{n-1}^{-}\left(\tilde{k}\right)-\tilde{\mu}}{2}-\tanh\frac{\tilde{E}_{n}^{+}\left(\tilde{k}\right)-\tilde{\mu}}{2}\right]\frac{\left(\chi_n^-\left(\tilde{k}\right)\right)^2\left(\chi_{n-1}^-\left(\tilde{k}\right)\right)^2}{\left(\tilde{E}_{n-1}^{-}\left(\tilde{k}\right)-\tilde{E}_{n}^{+}\left(\tilde{k}\right)\right)^2}\\
&+\frac{-e^2\tilde{\beta}T}{16\pi^2 v}\int d\tilde{k}\sum_{n=1}\left[\tanh\frac{\tilde{E}_{n-1}^{+}\left(\tilde{k}\right)-\tilde{\mu}}{2}-\tanh\frac{\tilde{E}_{n}^{-}\left(\tilde{k}\right)-\tilde{\mu}}{2}\right]\frac{\left(\chi_n^+\left(\tilde{k}\right)\right)^2\left(\chi_{n-1}^+\left(\tilde{k}\right)\right)^2}{\left(\tilde{E}_{n-1}^{+}\left(\tilde{k}\right)-\tilde{E}_{n}^{-}\left(\tilde{k}\right)\right)^2}\\
&+\frac{-e^2\tilde{\beta}T}{16\pi^2 v}\int d\tilde{k}\sum_{n=1}\left[\tanh\frac{\tilde{E}_{n-1}^{-}\left(\tilde{k}\right)-\tilde{\mu}}{2}-\tanh\frac{\tilde{E}_{n}^{-}\left(\tilde{k}\right)-\mu}{2}\right]\frac{\left(\chi_n^+\left(\tilde{k}\right)\right)^2\left(\chi_{n-1}^-\left(\tilde{k}\right)\right)^2}{\left(\tilde{E}_{n-1}^{-}\left(\tilde{k}\right)-\tilde{E}_{n}^{-}\left(\tilde{k}\right)\right)^2}.
\end{aligned} \tag{19}$$

and

$$\sigma_{xx}=\frac{e^2T}{v}\frac{\tilde{\beta}}{2\pi}\int\frac{d\tilde{\omega}}{2\pi}\frac{d\tilde{k}}{2\pi}\cosh^{-2}\frac{\tilde{\omega}}{2}\tilde{F}\left(\tilde{\omega},\tilde{k}\right), \tag{20}$$

where

$$\begin{aligned}
\tilde{F}\left(\tilde{\omega},\tilde{k}\right)=&\frac{1}{4}\sum_n\frac{(\chi_n^-(\tilde{k}))^2/\tilde{\tau}_n^+(\tilde{k})}{\left(\tilde{\omega}+\tilde{\mu}-\tilde{E}_n^+\left(\tilde{k}\right)\right)^2+\frac{1}{(\tilde{\tau}_n^+(\tilde{k}))^2}}\frac{(\chi_{n-1}^+(\tilde{k}))^2/\tilde{\tau}_{n-1}^+(\tilde{k})}{\left(\tilde{\omega}+\tilde{\mu}-\tilde{E}_{n-1}^+\left(\tilde{k}\right)\right)^2+\frac{1}{(\tilde{\tau}_{n-1}^+(\tilde{k}))^2}}\\
&+\frac{1}{4}\sum_n\frac{(\chi_n^-(\tilde{k}))^2/\tilde{\tau}_n^+(\tilde{k})}{\left(\tilde{\omega}+\tilde{\mu}-\tilde{E}_n^+\left(\tilde{k}\right)\right)^2+\frac{1}{(\tilde{\tau}_n^+(\tilde{k}))^2}}\frac{(\chi_{n-1}^-(\tilde{k}))^2/\tilde{\tau}_{n-1}^-(\tilde{k})}{\left(\tilde{\omega}+\tilde{\mu}-\tilde{E}_{n-1}^-\left(\tilde{k}\right)\right)^2+\frac{1}{(\tilde{\tau}_{n-1}^-(\tilde{k}))^2}}\\
&+\frac{1}{4}\sum_n\frac{(\chi_n^+(\tilde{k}))^2/\tilde{\tau}_n^-(\tilde{k})}{\left(\tilde{\omega}+\tilde{\mu}-\tilde{E}_n^-\left(\tilde{k}\right)\right)^2+\frac{1}{(\tilde{\tau}_n^-(\tilde{k}))^2}}\frac{(\chi_{n-1}^+(\tilde{k}))^2/\tilde{\tau}_{n-1}^+(\tilde{k})}{\left(\tilde{\omega}+\tilde{\mu}-\tilde{E}_{n-1}^+\left(\tilde{k}\right)\right)^2+\frac{1}{(\tilde{\tau}_{n-1}^+(\tilde{k}))^2}}\\
&+\frac{1}{4}\sum_n\frac{(\chi_n^+(\tilde{k}))^2/\tilde{\tau}_n^-(\tilde{k})}{\left(\tilde{\omega}+\tilde{\mu}-\tilde{E}_n^-\left(\tilde{k}\right)\right)^2+\frac{1}{(\tilde{\tau}_n^-(\tilde{k}))^2}}\frac{(\chi_{n-1}^-(\tilde{k}))^2/\tilde{\tau}_{n-1}^-(\tilde{k})}{\left(\tilde{\omega}+\tilde{\mu}-\tilde{E}_{n-1}^-\left(\tilde{k}\right)\right)^2+\frac{1}{(\tilde{\tau}_{n-1}^-(\tilde{k}))^2}}.
\end{aligned} \tag{21}$$

In the above, the dimensionless normalized scattering time $\frac{1}{2\tilde{\tau}_n^\lambda(\tilde{k})}$ is expressed by these normalized quantities as:

$$\frac{1}{\tilde{\tau}_n^\lambda(\tilde{k})} = \frac{1}{\tau_n^\lambda((\tilde{k}))T} = \tilde{N}\sum_{\gamma=\pm}\int d\tilde{k}'\Bigg\{\frac{1}{\left(\tilde{\mu}-\tilde{E}_{n-1}^\gamma\left(\tilde{k}'\right)\right)^2+1}\left[\frac{4(\mathcal{B}_{n,\lambda}^{n-1,\gamma}\left(\tilde{k},\tilde{k}'\right))^2}{\tilde{\beta}^2}+(\mathcal{A}_{n,\lambda}^{n-1,\gamma}\left(\tilde{k},\tilde{k}'\right))^2\right]$$
$$\times\left(\ln\frac{\tilde{\beta}/2+\tilde{K}^2(\tilde{k},\tilde{k}')}{\tilde{K}^2(\tilde{k},\tilde{k}')}+\frac{\tilde{K}^2(\tilde{k},\tilde{k}')}{\tilde{\beta}/2+\tilde{K}^2(\tilde{k},\tilde{k}')}-1\right)\Bigg\}$$
$$+\tilde{N}\sum_{\gamma=\pm}\int d\tilde{k}'\Bigg\{\frac{1}{\left(\tilde{\mu}-\tilde{E}_{n+1}^\gamma\left(\tilde{k}'\right)\right)^2+1}\left[\frac{4(\mathcal{B}_{n,\lambda}^{n+1,\gamma}\left(\tilde{k},\tilde{k}'\right))^2}{\tilde{\beta}^2}+(\mathcal{A}_{n,\lambda}^{n+1,\gamma}\left(\tilde{k},\tilde{k}'\right))^2\right]$$
$$\times\left(\ln\frac{\tilde{\beta}/2+\tilde{K}^2(\tilde{k},\tilde{k}')}{\tilde{K}^2(\tilde{k},\tilde{k}')}+\frac{\tilde{K}^2(\tilde{k},\tilde{k}')}{\tilde{\beta}/2+\tilde{K}^2(\tilde{k},\tilde{k}')}-1\right)\Bigg\}, \tag{22}$$

where $\tilde{N}=\frac{v^3}{\tilde{\varepsilon}_\infty^2}\frac{N_i}{T^3}$ is the normalized density of impurity, and $\tilde{K}(\tilde{k},\tilde{k}')=v^2K(k_z,k_z')/T^2$.

A. The low temperature case $T \ll \sqrt{v^2\beta_0}$

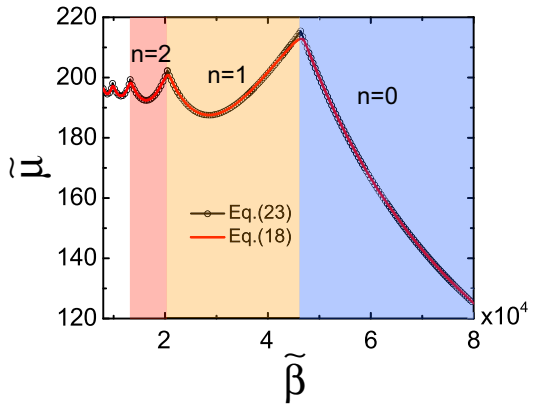

FIG. 2: The normalized chemical potential $\tilde{\mu}$ as a function of the normalized magnetic field $\tilde{\beta}\sim B$. The number n denotes the highest Landau level crossed by the chemical potential within the color highlighted region.

Here we assume the normalized carrier density as $\tilde{n}_0=10^7$. Then the chemical potential can be determined first by Eq.(18). On the other hand, since the temperature is low, the integral over the Fermi distribution functions can be evaluated by substituting the Fermi distribution by the Heaviside step function ($\frac{1}{e^{(E_n^+(\tilde{k}_z,\tilde{\beta})\pm\tilde{\mu})}+1}\approx\Theta(E_n^+(\tilde{k}_z,\tilde{\beta})\mp\tilde{\mu})$).

Then we obtain the equation determining the chemical potential as:

$$\tilde{\beta}\left[\tilde{\mu}+\sum_{n=1}^{N}2\sqrt{\tilde{\mu}^2-n\tilde{\beta}}\right]=\tilde{n}_0, \tag{23}$$

where N is the highest Landau level below the chemical potential.

In Fig. 2, the chemical potential determined by Eq.(23) is shown by the black curve with open circles. For the comparison, the numerical results based on Eq.(18), which has accounted the effect of temperature are presented by the red curve in the same figure. It turns out that $\tilde{\mu}$ changes with $\tilde{\beta}$ non-monotonously, and a clear increment of $\tilde{\mu}$ at the bottom of each Landau level is seen. The two methods give consistent results, except for some obvious temperature corrections at the bottom of each Landau level due to the high density of states.

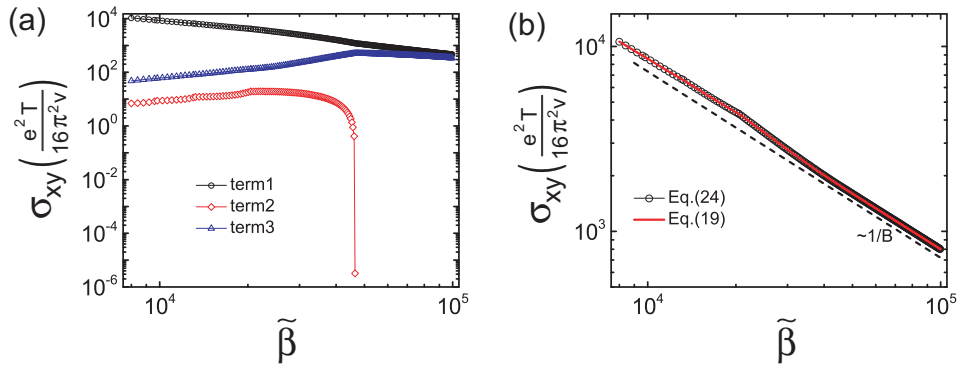

FIG. 3: (a) the plot of the three terms in Eq.(24) composing the Hall conductivity σ_{xy} as functions of $\tilde{\beta}$; (b) the Hall conductivity σ_{xy} as a function of $\tilde{\beta}$. The red solid line is obtained numerically based on Eq.(19), while the black curve with open circles is obtained under the low temperature approximation Eq.(24). The black dashed line presents the $1/B$ scaling.

Similarly, when T is small in compared with $\tilde{\beta}$, the Hall conductivity σ_{xy} can be further simplified to:

$$\sigma_{xy}=\underbrace{\frac{e^2\tilde{\beta}T}{8\pi^2 v}\sum_{n=1}^{N+1}b\int_{k_n^\mu}^{k_{n-1}^\mu}d\tilde{k}\frac{\left(\chi_n^-\left(\tilde{k}\right)\right)^2\left(\chi_{n-1}^+\left(\tilde{k}\right)\right)^2}{\left(\tilde{E}_{n-1}^+\left(\tilde{k}\right)-\tilde{E}_n^+\left(\tilde{k}\right)\right)^2}}_{\text{term1}}+\underbrace{\frac{e^2\tilde{\beta}T}{8\pi^2 v}\sum_{n=2}^{N+1}\int_{k_n^\mu}^{k_{n-1}^\mu}d\tilde{k}\frac{\left(\chi_n^-\left(\tilde{k}\right)\right)^2\left(\chi_{n-1}^-\left(\tilde{k}\right)\right)^2}{\left(\tilde{E}_{n-1}^-\left(\tilde{k}\right)-\tilde{E}_n^+\left(\tilde{k}\right)\right)^2}}_{\text{term2}}$$
$$+\underbrace{\frac{e^2\tilde{\beta}T}{8\pi^2 v}\sum_{n=1}^{N+1}\int_{k_n^\mu}^{k_{n-1}^\mu}d\tilde{k}\frac{\left(\chi_n^+\left(\tilde{k}\right)\right)^2\left(\chi_{n-1}^+\left(\tilde{k}\right)\right)^2}{\left(\tilde{E}_{n-1}^+\left(\tilde{k}\right)-\tilde{E}_n^-\left(\tilde{k}\right)\right)^2}}_{\text{term3}}, \tag{24}$$

where N denotes the highest Landau level crossed by the chemical potential, k_n^μ means the Fermi wave vector for the n Landau level, $b=1$ for $n=1$, and $b=2$ for other cases. The first term in Eq.(24) contains the process between positive Landau levels, while the last two terms involve the processes between the positive and negative Landau levels.

In Fig. 3(a), we plot the three parts of σ_{xy} as functions of $\tilde{\beta}$. When only the lowest Landau level is relevant, the second term simply gets vanishing, while both the first term and the third term provide significant contribution to the Hall conductivity σ_{xy}. Based on Eq.(24), with the chemical potential under the condition, the Hall conductivity σ_{xy} can be written as:

$$\sigma_{xy}=\frac{e^2\tilde{\beta}T}{8\pi^2 v}\left[\int_0^{k_0^\mu}d\tilde{k}\frac{\left(\chi_1^-(\tilde{k})\right)^2\left(\chi_0^+(\tilde{k})\right)^2}{\left(E_0^+\left(\tilde{k}\right)-E_1^+\left(\tilde{k}\right)\right)^2}+\int_0^{k_0^\mu}d\tilde{k}\frac{\left(\chi_1^+(\tilde{k})\right)^2\left(\chi_0^+(\tilde{k})\right)^2}{\left(E_0^+\left(\tilde{k}\right)-E_1^-\left(\tilde{k}\right)\right)^2}\right], \tag{25}$$

where the first term is the approximation taken by Abrikosov [27] containing the processes between the positive Landau levels, and the second term is from 'term3' in Eq.(24) containing the processes between the positive and negative Landau levels. When $\tilde{k}^2\ll\tilde{\beta}$, $\chi_1^-(\tilde{k})\approx\chi_1^+(\tilde{k})$, and the chemical potential is very close to the nodal point, which means $E_1^+-\mu\approx-(E_1^--\mu)$ or particle-hole symmetry preserves approximately. Therefore, when $\tilde{k}^2\ll\tilde{\beta}$, the first term is equal to the second term in Eq.(25), and the Abrikosov's approximation misses a factor 2 in the final result of σ_{xy}. Accordingly, in Fig. 3(a) with the increasing of $\tilde{\beta}$, the difference between 'term1' and 'term3' becomes smaller and smaller.

In Fig. 3(b), the Hall conductivity σ_{xy} obtained by the low temperature approximation (Eq.(24)) is shown by the black curve with circle symbols. The Hall conductivity σ_{xy} obtained by the direct numerical evaluation of Eq.(19) is shown by the red curve in the same figure for the comparison. It turns out that both methods give very good consistency. Moreover, a precise $1/B$ behavior is shown, when the condition $\mu \ll \sqrt{2v^2\beta}$, which was proposed in the seminar work by Abrikosov, is fulfilled. When $\tilde{\beta}$ is not large enough, the behavior of σ_{xy} deviates from $1/B$ slightly.

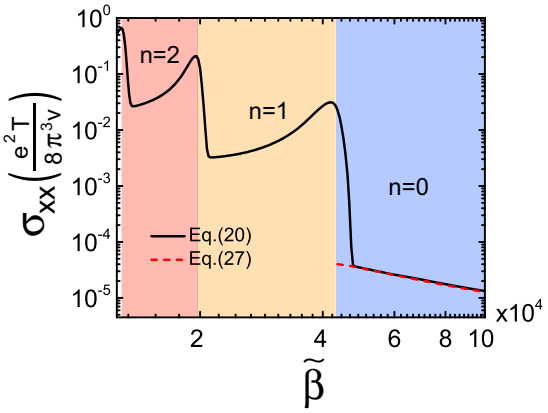

FIG. 4: The plot of the calculated longitudinal conductivity σ_{xx} versus the reduced magnetic field $\tilde{\beta}$. The number n denotes the highest Landau level crossed by the chemical potential within the color highlighted region.

At the same time, the longitudinal conductivity σ_{xx}, under the conditions that the temperature is low and the chemical potential crosses only the lowest Landau level, can be greatly simplified from Eq.(20):

$$\sigma_{xx} \approx \frac{e^2T\tilde{\beta}}{4\pi^2 v}\frac{(\chi_1^-(\tilde{k}_0^{\tilde{\mu}}))^2/\tilde{\tau}_1^+(\tilde{k}_0^{\tilde{\mu}})}{(\tilde{E}_1^+(\tilde{k}_0^{\tilde{\mu}})-\tilde{E}_0^+(\tilde{k}_0^{\tilde{\mu}}))^2}+\frac{e^2T\tilde{\beta}}{4\pi^2 v}\frac{(\chi_1^+(\tilde{k}_0^{\tilde{\mu}}))^2/\tilde{\tau}_1^-(\tilde{k}_0^{\tilde{\mu}})}{(\tilde{E}_1^-(\tilde{k}_0^{\tilde{\mu}})-\tilde{E}_0^+(\tilde{k}_0^{\tilde{\mu}}))^2}, \tag{26}$$

where $\tilde{k}_0^{\mu}$ is the Fermi energy for the $n=0$ Landau level, and $\tilde{\tau}_1^{\pm}$ is the reduced scattering time for the $n=\pm 1$ Landau level, which can be obtained from Eq.(22) under the same approximations:

$$\frac{1}{\tilde{\tau}_1^{\pm}(\tilde{k}_0^{\tilde{\mu}})} \approx \frac{\pi\tilde{N}}{\tilde{\beta}}(\chi_1^{\pm}(\tilde{k}_0^{\tilde{\mu}}))^2\left(\ln\frac{\tilde{\beta}+\tilde{\kappa}^2}{\tilde{\kappa}^2}+\frac{\tilde{\kappa}^2}{\tilde{\beta}+\tilde{\kappa}^2}-1\right), \tag{27}$$

where $\tilde{\kappa}=v\kappa/T$. Combining Eq.(25) and Eq.(26), we arrive at the expression of longitudinal conductivity under the

conditions mentioned above:

$$\sigma_{xx} \approx \frac{e^2 T\tilde{N}}{8\pi v}\frac{1}{\tilde{\beta}}\frac{4(\tilde{k}_0^{\tilde{\mu}})^2+2\tilde{\beta}}{(\tilde{k}_0^{\tilde{\mu}})^2+\tilde{\beta}}\left(\ln\frac{\tilde{\beta}+\tilde{\kappa}^2}{\tilde{\kappa}^2}+\frac{\tilde{\kappa}^2}{\tilde{\beta}+\tilde{\kappa}^2}-1\right). \tag{28}$$

It is easy to check that when $\mu \ll \sqrt{2v^2\beta}$, the longitudinal conductivity σ_{xx} is proportional to $1/\tilde{\beta} \propto 1/B$. Together with the $1/B$ behavior of σ_{xy}, the linear magnetoresistance is expected under these conditions, which is consistent with the observation of Abrikosov. In Fig. 4, the longitudinal conductivity σ_{xx} obtained numerically from Eq.(20) is plotted as a function of $\tilde{\beta}$. The conductivity shows a non-monotonous behavior, and at around the bottom of each Landau level a maximal in conductivity appears due to the high density of states. For the $n = 0$ case, σ_{xx} can be expressed by Eq.(27) in low temperature, which is plotted in the Fig. 4 as a comparison and agrees well with the numerical result based on Eq.(20).

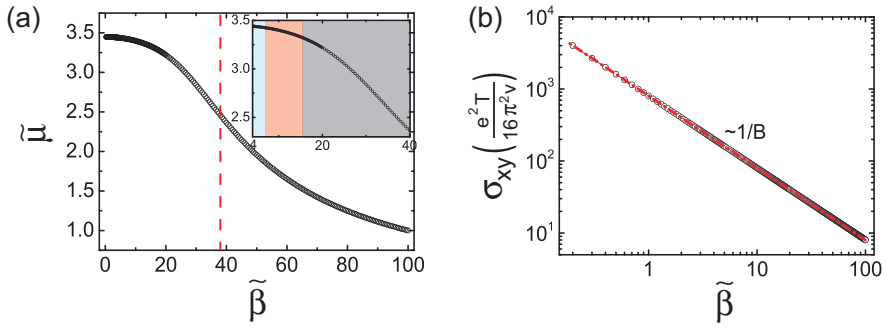

FIG. 5: (a) the normalized chemical potential $\tilde{\mu}$ versus $\tilde{\beta}$: the red dashed line denotes the boundary between $n = 0$ and $n = 1$ Landau levels, the black shielding region is corresponding to $n = 1$ Landau level, the red shielding region corresponds to $n = 2$ Landau level, and the blue shielding region is for $n = 3$ Landau levels. (b) the plot of the Hall conductivity σ_{xy} as a function of $\tilde{\beta}$. In the above calculations, the normalized carrier density is $\tilde{n}_0 = 10^2$.

B. The high temperature case $T \sim \sqrt{v^2\beta_0}$

To reduce the difficulties in numerical calculation, the normalized carrier density is set to be $\tilde{n}_0 = 10^2$. The relation between the normalized chemical potential and $\tilde{\beta} \sim B$ can be obtained through Eq.(18) and is plotted in Fig. 5(a). With the decreasing magnetic field, the chemical potential is found to increase monotonously. When the magnetic field approaches to $\tilde{\beta} = 0$, the normallized chemical potential gets saturated as expected. According to Eq.(23), the low-temperature boundary between the $n = 0$ Landau level and the $n = 1$ Landau level is about $\tilde{\beta} \approx 40$ (see the red dashed line in Fig. 5(a)). Approximately at the value, the increasing rate of $\tilde{\mu}$ with the decreasing magnetic field reaches the maximal. After that ($\tilde{\beta} < 40$), the increasing rate of $\tilde{\mu}$ with the decreasing magnetic field gradually decreases. During the process of decreasing magnetic field, $\tilde{\beta}$ passes a few low-temperature boundaries between neighbored Landau levels (see the inset of Fig. 5(a)), but due to the temperature smearing the renormaized chemical potential $\tilde{\mu}$ does not show dramatic increment like what are shown in low temperature case (see Fig.2). Under the situation $T \sim \sqrt{v^2\beta_0}$, the Hall conductivity σ_{xy} can be calculated by Eq.(19) numerically, and the relation between σ_{xy} and $\tilde{\beta}$ is plotted in Fig. 5(b). It turns out that the Hall conductivity shows the $1/B$ behavior over the whole parameter regime. Comparing with its low-temperature behavior shown in Fig. 3(b), the temperature effect further smears out the non-$1/B$ behaviors.

Further we study the dependence of the longitudinal magneto-conductivity σ_{xx} on the external magnetic field, when the effect of temperature is important. To make the calculation as accurate as possible, about 2000 Landau levels are used in the summation in Eq.(21). In Fig. 6(a), the longitudinal conductivity σ_{xx} is plotted as a function of $\tilde{\beta}$. With the decreasing magnetic field, the behavior of σ_{xx} shows five regimes: 1. when the chemical potential locates at

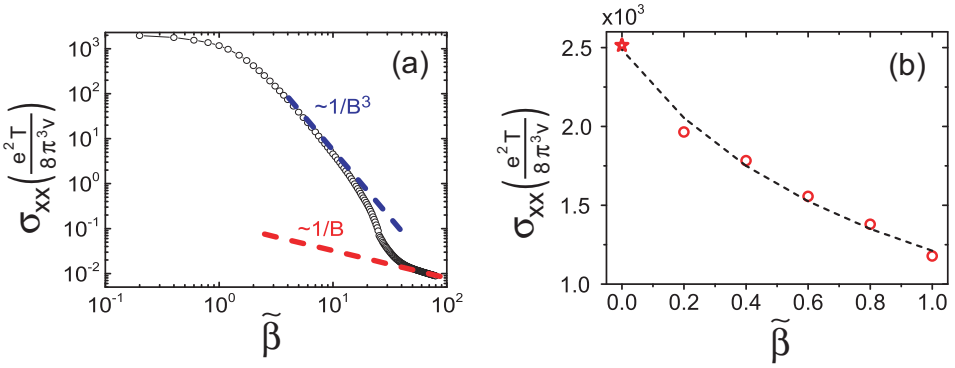

FIG. 6: The magnetic field dependence of the longitudinal conductivity σ_{xx}: (a) the plot of σ_{xx} as a function of $\tilde{\beta}$; (b) the closeup of the magnetic field dependence behavior close to $\tilde{\beta} = 0$: the red circles are the calculated longitudinal magneto-conductivity, when $\tilde{\beta} \neq 0$; the red star is the calculated longitudinal conductivity σ^0_{xx}; the black dashed curve is the fitted following the Lorentzian form $\sigma_{xx} = \frac{\sigma^0_{xx}}{1+(\omega_c\tau)^2}$.

the zeroth Landau level, the longitudinal magneto-conductivity σ_{xx} shows a $1/B$ behavior. Together with the $1/B$ behavior of Hall conductivity, within this parameter regime, linear magnetoresistance is expected; 2. with the further decrease of magnetic field, the magnetic field dependence of σ_{xx} crosses over from $1/B$ to $1/B^3$; 3. within a broad regime around $\tilde{\beta} = 10$, the longitudinal magneto-conductivity σ_{xx} shows $1/B^3$ accidentally (the explanation of $1/B^3$ behavior within this parameter regime is given in the appendix A.); 4. when $\tilde{\beta} < 5$, σ_{xx} deviates from $1/B^3$ and crossover to the Lorentzian form $\sigma_{xx} = \frac{\sigma^0_{xx}}{1+(\omega_c\tau)^2}$; 5. when $\tilde{\beta} < 1$, the behavior of σ_{xx} can be fitted by the Boltzmann result $\sigma_{xx} = \frac{\sigma^0_{xx}}{1+(\omega_c\tau)^2}$ (see Fig. 6(b)). The fitted longitudinal conductivity is $\sigma^0_{xx} = 2485.7e^2T/(8\pi^3 v)$, which is closed to the calculated value $\sigma^0_{xx} = 2513.9e^2T/(8\pi^3 v)$.

C. Magnetoresistance: a comparison with experimental data

The experimentally relevant quantity longitudinal magnetoresistance ρ_{xx} relates with σ_{xx} and σ_{xy} as:

$$\rho_{xx} = \frac{\sigma_{xx}}{\sigma_{xx}^2 + \sigma_{xy}^2}.$$

We plot the magnetoresistance ρ_{xx} as a function of $\tilde{\beta}$ for a typical carrier density $\tilde{n}_0 = 2 \times 10^3$ in Fig. 7(a). The carrier density is chosen so that all the features discussed in the previous sections can manifest. Based on the discussions in the pervious sections, the magnetoresistance ρ_{xx} is expected to show different behaviors in three different regimes: *regime I.* when the magnetic field is high enough, the chemical potential is pushed down to intersect only with the zeroth Landau level, and the magnetoresistance ρ_{xx} would increase with the external field linearly, which is corresponding to the high-field regime of the low-temperature case (see Fig. 4); *regime II.* when the magnetic field is smaller but $\sqrt{v^2\beta_0}$ still larger than the temperature T, the magnetoresistance ρ_{xx} would show oscillations, which is consistent with the low-field regime of the low temperature case (see Fig. 4); *regime III.* when the magnetic field is further smaller and $\sqrt{v^2\beta_0}$ is comparable with the temperature T, the oscillation of magnetoresistance ρ_{xx} is smeared out by the thermal effect, which is corresponding to the low-field regime of the high-temperature case (see Fig. 6(a)).

As a comparison, the experimental data [26] of magnetoresistance ρ_{xx} as a function of magnetic field B is plotted in Fig. 7(b). From the experimental data, it can be seen that within *regime I* the magnetoresistance increases linearly with the magnetic field, which is consistent with the results based on self-energy approximation. However, though the oscillation of ρ_{xx} can be observed in *regime II* and the smearing effect of temperature can be seen in the subsequent *regime III*, a qualitative difference between experimental data and the results based on self-consistent approximation can be identified clearly. The experimental data with the increment of external field increases monotonously, but

ρ_{xx} obtained from the self-energy approximation shows a complex non-monotonous behavior with the increment of magnetic field.

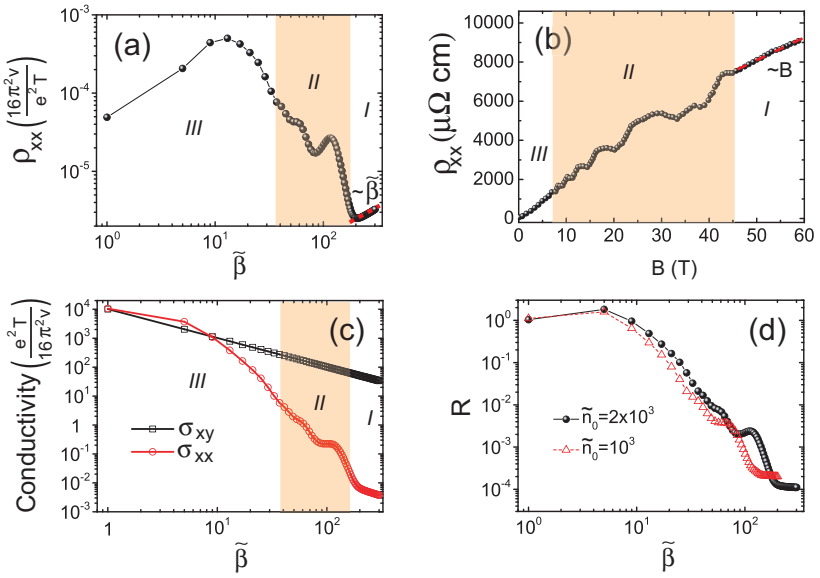

FIG. 7: (a) the plot of ρ_{xx} as a function of $\tilde{\beta}$ for a typical carrier densities $\tilde{n}_0 = 2 \times 10^3$; (b) the experimental data of ρ_{xx} as a function of B extracted from ref. [26]; (c) the plot of σ_{xx} and σ_{xy} as functions of $\tilde{\beta}$ for carrier density $\tilde{n}_0 = 2 \times 10^3$; (d) the plot of ratio $R = \sigma_{xx}/\sigma_{xy}$ as a function of $\tilde{\beta}$ for two different carrier density: the black curve with dot symbols is for $\tilde{n}_0 = 2 \times 10^3$, and the red curve with triangle symbols is for $\tilde{n}_0 = 10^3$. For the clarity, in (a), (b) and (c) the *regime II*, where oscillation of ρ_{xx} can be observed, is highlighted in orange.

Within the self-energy approximation, Hall conductivity σ_{xy} generally shows a $1/\tilde{\beta}$ behavior. However, the behavior of longitudinal conductivity σ_{xx} depends on the position of chemical potential and the ratio between $\sqrt{v^2\beta_0}$ and T. In Fig. 7(c), we plot both σ_{xy} and σ_{xx} as functions of $\tilde{\beta}$ for a carrier density $\tilde{n}_0 = 2 \times 10^3$. It can be seen that in the presence of low magnetic field σ_{xx} is comparable with σ_{xy}, but with the increment of magnetic field the ratio between longitudinal and Hall conductivity $R = \sigma_{xx}/\sigma_{xy}$ becomes smaller and smaller until the chemical potential intersects only the $n = 0$ Landau level. This can be seen more clearly from the black curve with dot symbols in Fig. 7(d). The

non-monotonous behavior of the ratio R is mainly due to the complex behavior of σ_{xx} and gives the explanation of the behavior of ρ_{xx} obtained from the self-energy approximation. The change of carrier density would not affect the qualitative behavior of R (see the red curve with triangular symbols in Fig. 7(d)), neither it changes the behavior of ρ_{xx} qualitatively.

IV. DISCUSSION AND CONCLUSION

In this work, we studied the magneto-transport based on a low-energy effective model of a single Weyl node within the self-energy approximation for charged impurities under the Landau representation. Though the Weyl nodes should appear in pairs, as long as one focus on the bulk and is not interested in the interplay between different nodes, a single node model is enough to obtain reasonable results. In our case, the effect of multi-node can be accounted simply by multiplying the results of single node model by the number of nodes. The results present here are valid, when the sample is clean with $\tau \ll \sqrt{v^2\beta_0}$ and the smearing of Landau level caused by disorder can be ignored. On the other hand, the effect of temperature and chemical potential on the transport properties were examined carefully.

In the low temperature limit ($T \ll \sqrt{v^2\beta_0}$), within the self-energy approximation, the chemical potential varies with the change of external magnetic field non-monotonously, when the carrier density in the system is a constant. In this limit, the Hall conductivity basically follows the $1/B$ behavior except for a small derivation when chemical potential crosses a Landau level band bottom. For the longitudinal magneto-conductivity, the following magnetic field dependence appears: it shows $1/B$ behavior, if the chemical potential intersects only with the $n = 0$ Landau level; On the other hand, the longitudinal magneto-conductivity shows the 'step-like' structure and is with steep increasing at the edges of Landau levels due to the high density of states, when the the chemical potential locates at $n \geq 1$ Landau

levels.

When the temperature is comparable with the gap between Landau levels ($T \sim \sqrt{v^2\beta_0}$), the chemical potential increases with the decreasing external magnetic field, and the Hall conductivity within this parameter regime shows nicely the $1/B$ behavior. In this parameter regime, the magnetic field dependence behavior of longitudinal magneto-conductivity can be divided into five regimes. The same with the low temperature case, the $1/B$ behavior appears, when the chemical potential intersects only with the $n = 0$ Landau level. Therefore, within the self-energy approximation, no matter the temperature is high or low, the linear magneto-resistance can appear robustly, when the magnetic field is large enough to pull the chemical potential intersecting with the $n = 0$ Landau level only. Also an accidental $1/B^3$ behavior happens within a wide region around $\tilde{\beta} = 10$, when the external magnetic field is tuning. When the magnetic field is very small ($\tilde{\beta} < 1$), the magneto-conductivity scales with the magnetic field in the Lorentzian form. These three regions are connected by two crossover regions.

The magnetoresistance ρ_{xx} obtained within the Born and self-energy approximation can be generally divided into three regimes: Linear magnetoresistance appears in the high-field regime (*regime I* in Fig. 7); the quantum oscillation of magnetoresistance can be seen in the middle-field regime (*regime II* in Fig. 7); the oscillation of magnetoresistance is smeared out by the thermal effect in the low-field regime (*regime III* in Fig. 7). The features mentioned above can indeed seen in the experimental data [26]. However, the magnetoresistance obtained from self-energy approximation increases with magnetic field non-monotonously, while the measured magnetoresistance generally shows a monotonous increment [26]. Moreover, in experiments the magnetoresistance appears to be linear and associated with quantum oscillations [23, 26], which indicates that the linear magneto-resistance can appear even when the chemical potential intersects with higher Landau levels. We conclude that the Born and self-energy approximation of this model does

not explain the linear and non-saturated magnetoresistance in experiments. Whether the classical argument of ref.[29] can be obtained in a diagrammatic treatment is an open question.

Acknowledgments

PAL would like to acknowledge the support of DOE under grant DE-FG01-03-ER46076. He also thank the hospitality of the Institute of Advanced studies at the Hong Kong University of Science and Technology. KTL thanks the support of HKRGC and Croucher Foundation through HKUST3/CRF/13G, 602813, 605512, 16303014 and Croucher Innovation Grant.

Appendix: The accidental $1/B^3$ behavior in high temperature

The $1/B^3$ scaling around $\tilde{\beta} = 10$ is an accidental consequence involving many Landau levels. In what follows, we try to provide more information about it. Then we focus on the contribution to the longitudinal conductivity σ_{xx} from each Landau level for $\tilde{\beta} \in [4, 10]$. In Fig. 7(a), σ_{xx} contributed by each Landau level under different $\tilde{\beta}$ is plotted. As it is expected, within this region the maximal contribution comes from the Landau levels, where chemical potential cuts. The temperature indeed play roles by making the Landau levels around to contribute significantly. From the calculation, we can identify that about 20 Landau levels make important contributions. Another feature is that the contribution of each Landau level increases with the decreasing magnetic field.

On the other hand, the scaling of the contribution of each Landau level with $\tilde{\beta}$ also depends on the position of chemical potential. To demonstrate it, we we plot the longitudinal magneto-conductivity contributed by each Landau level in Fig. 7(b). From the plot, we notice that the more distance away from the chemical potential, the more quickly

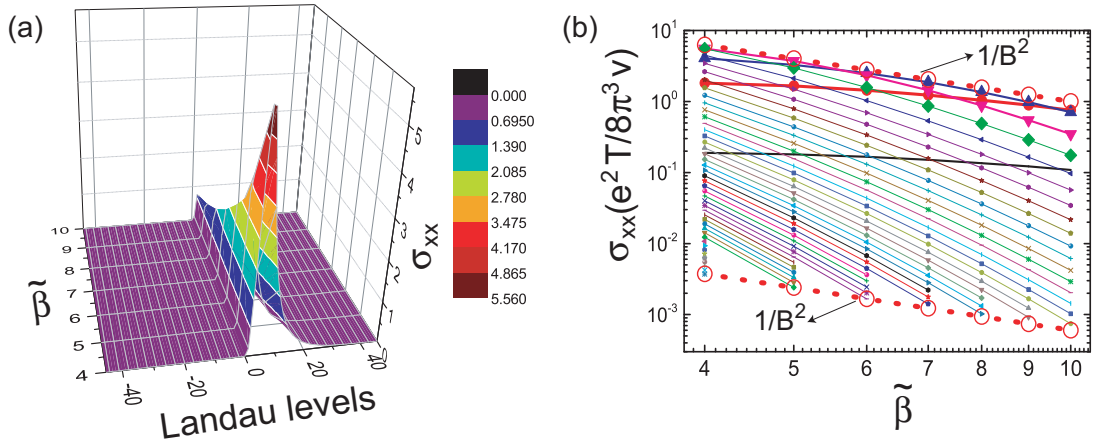

FIG. 8: (a) the contribution of each Landau level to the longitudinal magneto-conductivity σ_{xx}, when the magnetic field changes within $\tilde{\beta} \in [4, 10]$; (b) the contribution of each Landau level to the longitudinal magneto-conductivity versus magnetic field $\tilde{\beta}$: the black curve without symbol is the contribution from the zeros Landau level, the red curve with round dot presents the contribution from the $n = 1$ Landau level, the blue curve with upward triangle is for the contribution from $n = 2$ Landau level, the pink curve with downward triangle is for the $n = 3$ Landau level, and green curve with diamond symbol is for $n = 4$ Landau levels. In (a), the unit of σ_{xx} is the same with that in (b).

the contribution of the Landau level decays with increasing magnetic field. As a result, the $1/B^3$ behavior is very hard to understand based on the behavior of a single Landau level.

However, one can understand this from the other point of view. For this whole branch of Landau levels, one can find the maximal and minimal values of the contributions, which fulfill the $1/B^2$ behaviors very nicely (see the red dashed lines with open circle symbols in Fig. 7(b)). On the other hand, due to the thermal factor $\cosh^{-2}(E_n - \mu)/2T$, only the states within the energy gap $\mu - E_c < E_n < \mu + E_c$ gives significant contributions to the conductivity. Out of the range, $\cosh^{-2}(E_n - \mu)/2T$ is small enough, so we can drop those contributions. Then we can see that the number of Landau level involving is given by $N \approx (\tilde{\mu} + E_c)^2/\tilde{\beta} + (\tilde{\mu} - E_c)^2/\tilde{\beta} \sim 1/\tilde{\beta}$. Considering that the gap between Landau

levels are slowly changing, then the total longitudinal magneto-conductivity can be approximated given by:

$$\sigma_{xx} \approx 1/2\,[\max \sigma_{xx}^{n} + \min \sigma_{xx}^{n}]\,N \sim 1/\tilde{\beta}^{3}. \tag{1}$$

Based on the above analysis, we notice that though $1/B^3$ behavior can indeed appear for different carrier densities, but this behavior is just a part of crossover from the $1/B$ behavior in the $n = 0$ Landau level.

---

[1] K. S. Novoselov *et al*, Science **306**, 666 (2004).

[2] A. H. Castro Neto, F. Guinea, N. M. R. Peres, K. S. Novoselov, and A. K. Geim, Rev. Mod. Phys. **81**, 109 (2009).

[3] S. Das Sarma, S. Adam, E. H. Hwang, and E. Rossi, Rev. Mod. Phys. **83**, 407 (2011).

[4] V. N. Kotov, B. Uchoa, V. M. Pereira, F. Guinea, and A. H. Castro Neto, Rev. Mod. Phys. **84**, 1067 (2012).

[5] Y. Zhang, Y. Tan, H. L. Stormer, and P. Kim, Nature **438**, 201 (2005).

[6] M. O. Goerbig, Rev. Mod. Phys. **83**, 1193 (2011).

[7] Z. Wang *et al*, Phys. Rev. B **85**, 195320 (2012).

[8] Z. Wang, H. Weng, Q. Wu, X. Dai, and Z. Fang, Phys. Rev. B **88**, 125427 (2013).

[9] S. Xu *et al*, Science **347**, 294 (2015).

[10] B. J. Yang, and N. Nagaosa, Nat. Com. **5**, 4898 (2014).

[11] S. Xu *et al*, Science **349**, 613 (2015).

[12] S. Xu *et al*, Nat. Phys. **11**, 748 (2015).

[13] H. Weng, C. Fang, Z. Fang, B. A. Bernevig, and X. Dai, Phys. Rev. X **5**, 011029 (2015).

[14] X. Wan, A. M. Turner, A. Vishwanath, and S. Y. Savrasov, Phys. Rev. B **83**, 205101 (2011).

[15] A. A. Burkov, and L. Balents, Phys. Rev. Lett. **107**, 127205 (2011).

[16] S. L. Adler, Phys. Rev. **177**, 2426 (1969).

[17] J. S. Bell, and R. Jackiw, Nuovo Cimento A **60**, 47 (1969).

[18] V. Aji, Phys. Rev. B **85**, 241101 (2012).

[19] D. T. Son, and B. Z. Spivak, Phys. Rev. B **88**, 104412 (2013).

[20] C. X. Liu, P. Ye, and X. L. Qi, Phys. Rev. B **87**, 235306 (2013).

[21] S. A. Parameswaran, T. Grover, D. A. Abanin, D. A. Pesin, and A. Vishwanath, Phys. Rev. X **4**, 031035 (2014)

[22] X. Huang *et al*, Phys. Rev. X **5**, 031023 (2015).

[23] T. Liang *et al*, Nat. Mat. **14**, 280 (2015).

[24] J. Feng *et al*, Phys. Rev. B **92**, 081306 (2015).

[25] M. Novak, S. Sasaki, K. Segawa, and Y. Ando, Phys. Rev. B **91**, 041203 (2015).

[26] Y. Zhao *et al*, Phys. Rev. X **5**, 031037 (2015).

[27] A. Abrikosov, Phys. Rev. B, **58**, 2788 (1998).

[28] J. Klier, I. V. Gornyi, A. D. Mirlin, Phys. Rev. B **92**, 205113 (2015).

[29] J. C. W. Song, G. Refael, and P. A. Lee, Phys. Rev. B **92**, 180204 (2015).

[30] D. A. Pesin, E. G. Mishchenko, and A. Levchenko, Phys. Rev. B **92**, 174202 (2015).